

Cost effective combined axial fan and throttling valve control of ventilation rate

C.J. Taylor ¹

P.A. Leigh, A. Chotai, P.C. Young ²

E. Vranken, D. Berckmans ³

This paper is a postprint of a paper submitted to and accepted for publication in IEE Proceedings Control Theory and Applications and is subject to Institution of Engineering and Technology Copyright. The copy of record is available at IET Digital Library. [IEE Proceedings Control Theory and Applications **151**, 5, 577–584, 2004]

¹Engineering Department, Lancaster University, Lancaster, LA1 4YR, UK

²Department of Environmental Science, Lancaster University, UK

³Lab. for Agricultural Buildings Research, Katholieke Universiteit Leuven, Belgium

Abstract

This paper is concerned with Proportional-Integral-Plus (PIP) control of ventilation rate in mechanically ventilated agricultural buildings. In particular, it develops a unique fan and throttling valve control system for a $22m^3$ test chamber, representing a section of a livestock building or glasshouse, at the Katholieke Universiteit Leuven. Here, the throttling valve is employed to restrict airflow at the outlet, so generating a higher static pressure difference over the control fan. In contrast with previous approaches, however, the throttling valve is directly employed as a second control actuator, utilising airflow from either the axial fan or natural ventilation. The new combined fan/valve configuration is compared with a commercially available PID-based controller and a previously developed scheduled PIP design, yielding a reduction in power consumption in both cases of up to 45%.

Keywords

Agriculture; identification; control system design; model-based control; PIP control; PID control

1 Introduction

Ventilation rate is one of the most significant inputs in the control of microclimate surrounding plants or animals within the majority of agricultural buildings, including livestock housing, glasshouses and storage warehouses; see e.g. [1, 2, 3, 4]. For example, without adequate fresh air supply within a livestock enclosure, animal comfort and welfare are drastically reduced, especially during high density occupation by poultry, pigs or cattle, where excessive levels of moisture, heat and internal gases are generated. For this reason, the lack of effective ventilation rate control is a major cause of production losses and health problems in modern livestock buildings.

To date, the most common type of controllers used in agricultural buildings are derived from the ubiquitous Proportional-Integral-Derivative (PID) algorithms; e.g. [5, 6]. In this regard, the Proportional-Integral-Plus (PIP) controller considered in the present paper, can itself be interpreted as a logical extension of conventional PI/PID controllers, but with inherent model-based predictive control action [7]. Here, a Non-Minimal State Space (NMSS) model is formulated so that full state variable feedback control can be implemented directly from the measured input and output signals of the controlled process, without resort to the design and implementation of a deterministic state reconstructor or a stochastic Kalman filter [8]. Such PIP control sys-

tems have been successfully implemented in a wide range of applications, including the control of ventilation rate in a 22m³ laboratory test installation at the Katholieke Universiteit Leuven [9, 10].

In the latter regard, it should be noted that the desired airflow rate within agricultural buildings is typically set at a relatively low level. It is reasonably straightforward to maintain these low airflow rates (even in open loop) when the system is undisturbed. In practice, however, pressure disturbances caused by variations in wind speed outside the building, coupled with eddy currents or thermals inside, have a significant influence on the ventilation rate produced by an axial fan. In fact, at low ventilation rates, the air velocity vectors in the neighbourhood of the fan can be very turbulent, resulting in a fluctuating ventilation rate that is unsuitable for maintaining the environmental requirements (temperature, humidity, gas concentration) and the welfare of the animals within the building.

For this reason, a throttling valve has been developed to provide a second control actuator to the Leuven test chamber, as illustrated in Fig. 1. The radial blades of this valve (or vortex damper) can rotate through 90 degrees. At low ventilation rates, the valve is employed to restrict airflow through the chamber, so generating a higher static pressure difference over the control fan. For example, [10] consider the design and implementation of a gain scheduled PIP algorithm that activates the throttling valve when the ventilation rate

falls below $1000\text{m}^3/\text{h}$. For this preliminary design, the valve is always closed by a predetermined amount (60%) in order to help stabilise the airflow. The approach yields good control over a wide range of operating conditions when compared with a commercially available PID design. Of course, when the PIP or PID algorithms restrict the airflow in this way, the axial fan inevitably consumes more power in order to maintain a given ventilation rate.

By contrast, the present paper develops a PIP algorithm for active control of the throttling valve itself. Here, on-line adjustments are made to the blade angle at each control sample, in order to directly regulate the ventilation rate. The necessary airflow is generated either by the PIP controlled axial fan or, where appropriate, by natural ventilation caused by temperature gradients and wind outside the building. A simple rule-based algorithm switches control back to the fan when the throttling valve is no longer effective.

Following a brief description of the test chamber in Section 2, the modelling and control methodologies are developed in Sections 3 and 4 respectively. In Section 5, the new fan and throttling valve configuration is compared with previously developed controllers that use the same control actuators. Since microclimate control typically amounts to circa 15% of the production costs [4], the study pays particular attention to the relative power consumption of the various algorithms. Finally, the conclusions are given in Section 6.

2 Experimental chamber

The research discussed here is based on data collected from an instrumented ventilation test chamber at the Laboratory for Agricultural Buildings Research of the Katholieke Universiteit Leuven (Fig. 1). This facility has been designed to represent a section of a livestock building or glasshouse. Air is extracted from the chamber by an axial fan (diameter 0.45m), while a ventilation rate sensor (certified accuracy $50\text{m}^3/\text{h}$) is used for continuous feedback control.

A throttling valve alongside the ventilation rate sensor is utilised to restrict outflow. The radial blades can rotate from 0 to 90 degrees, i.e. ranging between perpendicular (fully closed) and parallel (fully open) to airflow direction. The power consumption of the throttling valve is insignificant in comparison to the fan. At the other side of the pressure chamber a second fan is used to create a dynamic pressure difference over the pressure chamber, thus simulating wind disturbances and natural ventilation.

Although not required for on-line control, static pressure differences over the control fan are measured with a differential pressure sensor that is automatically calibrated at the start of each experiment against a reference pressure sensor. Such measurements are particularly useful when specifying an appropriate signal to the disturbance fan in order to compare different

control strategies. Here, the voltage applied to the disturbance fan is adjusted by trial and error in a series of open loop experiments, in order to match the pressure differences observed on the external walls of a real building. As discussed in more detail by [4], this allows a realistic disturbance fan signal to be obtained from wind speed measurements. The present study utilises wind and pressure data collected at Silsoe Research Institute on a windy day with a mean wind speed of 4m/s [11].

The disturbance fan can also be utilised to represent any natural ventilation present in the system. Convenience and cost factors ensure that many farms install fans into the sidewall. This is a prominent feature of livestock farming in the low countries of Europe, including Belgium and Holland, where numerous farms are built along the coast of the North Sea and so are subjected to strong prevailing westerly winds. Furthermore, the ‘chimney effect’ tends to produce natural ventilation, especially when there is a temperature difference between inside and outside the building. In the latter case, warm air will be drawn from the interior towards any chimney structure, setting up a natural air-circulation without an electro/mechanical fan to drive it. In the case of the test chamber, the disturbance fan provides an airflow that is similarly independent of the main (control) fan.

2.1 Power curves

The steady state relationship between airflow rate and the potential voltage applied to the control fan is illustrated in Fig. 2 (circles), which takes the form of a conventional non-linear ‘S’ shaped curve. Here, a flexible logistic growth function has been numerically fitted to the data (in a least squares sense) in order to better highlight the relationship between these variables.

It should be pointed out that no airflow is produced below a certain potential voltage due to the motor characteristics of the fan, i.e. a certain threshold voltage is required to start the blades turning. In both Fig. 2 and the later analysis, the voltage is expressed as a percentage, where 0% represents this threshold and 100% is the maximum voltage normally applied.

The triangular data points in Fig. 2 are obtained for a partially closed throttling valve, illustrating the reduced ventilation rates when compared to the fully open valve case, for a given control fan setting. Here, the applied input to the throttling valve similarly ranges from 0% (valve fully open) to 100% (fully closed). In the case of the triangular data data points, the throttling valve input is 60%. It is clear from Fig. 2 that closing the valve increases operating costs for the control fan, since a higher voltage is required to maintain a given airflow.

Finally, the solid and dashed thick traces in Fig. 2 are for logistic growth

functions fitted to the steady state relationship between airflow rate and the applied voltage to the *throttling valve*. For the dashed trace, the control fan is turned off and the airflow is entirely provided by the disturbance fan operating at 40% power. For example, with the throttling valve blades turned parallel to the airflow, the mean ventilation rate is $3380\text{m}^3/\text{h}$. The solid trace is obtained with the disturbance fan turned off and 20% voltage applied to the control fan, yielding ventilation rates up to $1000\text{m}^3/\text{h}$.

These power curves suggest that, for a potential airflow generated by either the axial fan or an external disturbance, the ventilation rate may be regulated (reduced) by adjustment of the throttling valve. Of course, the set point reachable in such cases is constrained by the external force driving the airflow. In this regard, note that when the voltage applied to the valve exceeds $\approx 95\%$, the airflow sometimes becomes unstable because the outlet from the chamber is almost entirely blocked, hence the power curves are not graphed beyond this point.

3 System identification and estimation

In order to develop a PIP control algorithm, a linearised representation of the system is required. Even for non-linear systems, the essential small perturbation behaviour can usually be approximated well by simple linearised Trans-

fer Function (TF) models. For the purposes of the present paper, therefore, the discussion is limited to the following linear, single-input, single-output (SISO) discrete-time system,

$$y(k) = \frac{b_1 z^{-1} + \dots + b_m z^{-m}}{1 + a_1 z^{-1} + \dots + a_n z^{-n}} u(k) = \frac{B(z^{-1})}{A(z^{-1})} u(k) \quad (1)$$

where $y(k)$ is the ventilation rate (m^3/h) and $u(k)$ is the voltage applied to either the control fan or the throttling valve, expressed as a percentage in both cases, while $A(z^{-1})$ and $B(z^{-1})$ are appropriately defined polynomials in the backward shift operator z^{-1} , i.e. $z^{-i}y(k) = y(k-i)$. For convenience, any pure time delay of $\delta > 1$ samples can be accounted for by setting the $\delta-1$ leading parameters of the $B(z^{-1})$ polynomial to zero, i.e. $b_1, \dots, b_{\delta-1} = 0$.

In the PIP approach to control system design, it is recommended that the identification and estimation analysis should utilise the optimal Refined Instrumental Variable (RIV) or Simplified Refined Instrumental Variable (SRIV) algorithms [12, 13], since they are often more robust to noise model specification than commercial alternatives that require concurrent estimation of a noise model.

For a given physical system, an appropriate model structure first needs to be identified, i.e. the most appropriate values for the triad $[n, m, \delta]$. The two main statistical measures employed to help determine these values are the co-

efficient of determination R_T^2 , based on the response error; and YIC (Young's Information Criterion), which provides a combined measure of model fit and parametric efficiency, with large negative values indicating a model which explains the output data well, without over-parameterisation [13].

An important variable in the recursive estimation equations is the parameter covariance matrix $\mathbf{P}^*(k)$, which is the inverse of the Instrumental Cross-Product Matrix [see e.g. 14] scaled by the estimated noise variance. The standard errors on the parameter estimates may be computed from the diagonal elements of $\mathbf{P}^*(k)$. Also, $\mathbf{P}^*(k)$ provides an estimate of the uncertainty associated with the model parameters which can be employed in subsequent Monte Carlo analysis (see Section 4.5 below).

Finally, note that these statistical tools and associated estimation algorithms have been assembled as the CAPTAIN toolbox within the Matlab® software environment (www.es.lancs.ac.uk/cres/captain). The authors can be contacted for further details about the toolbox.

3.1 Control model for the axial fan

The paper discusses the design of PIP control systems for ventilation rate, based on a sampling rate of 2 seconds. Experimentation reveals that such a sampling rate yields a good compromise between a fast response and a

desirable low order model and control algorithm.

In order to identify the dominant dynamics of the main fan for a given operating condition, the disturbance fan is turned off, the throttling valve is set to fully open and airflow data are collected for 10% step changes in the applied voltage. In this case, the SRIV algorithm combined with the YIC and R_T^2 identification criteria suggest that a first order TF model with 3 samples time delay provides the best explanation of the data across a wide range of operating conditions [10]. In particular, with the fan operating in the middle range of airflow rates shown in Fig. 2 (2000-3000m³/h), the SRIV algorithm yields the following discrete-time TF model with $R_T^2 = 0.9866$ and YIC = -11.1,

$$y(k) = \frac{79.71z^{-3}}{1 - 0.4401z^{-1}}u_1(k) \quad (2)$$

where $u_1(k)$ is the applied voltage to the main fan.

3.2 Control model for the throttling valve

For the Leuven test chamber, the airflow stability problems discussed above typically occur for ventilation rates below 1000m³/h. For this reason, the control algorithm proposed in the present paper utilises the throttling valve when the applied voltage to the control fan drops to 20%. To derive an

appropriate TF model for the throttling valve, therefore, open loop experiments are conducted with the fan voltage set to a constant input of 20%. In this case, the ventilation rate is largely unaffected until the throttling valve applied voltage is greater than $\approx 30\%$ (refer to the thick solid trace in Fig. 2).

However, an approximate linear relationship exists between the throttling valve voltage and steady state ventilation rate, when the former is in the range 40% to 90%. In fact, a TF model with a similar structure to equation (2) provides a very good fit to experimental data across this range of operating conditions. For example, in the typical experiment illustrated by Fig. 3, the SRIV algorithm yields the following TF model with $R_T^2 = 0.9907$ and YIC = -12.3,

$$y(k) = \frac{-3.63z^{-3}}{1 - 0.7301z^{-1}}u_2(k) \quad (3)$$

where $u_2(k)$ is the applied voltage to the throttling valve. Note that the negative numerator parameter correctly implies that closing the valve restricts the airflow rate.

4 NMSS/PIP Control

The methodological approach follows from earlier research [7, 8], in which Non-Minimum State-Space (NMSS) models are formulated so that, in the

deterministic situation, full state feedback control can be implemented directly from the measured input and output signals of the controlled process, without resort to the design and implementation of a state reconstructor (or observer). As shown below, the approach automatically accomodates the mutiple-time delays observed in both the throttling valve and axial fan actuators, and yields a Proportional-Integral-Plus (PIP) design that is naturally robust to uncertainty, eliminating the need for measures such as loop transfer recovery.

The proposed fan/valve configuration employs independently designed, single input, single output (SISO) controllers to determine the applied voltage to the axial fan and the throttling valve. Although the NMSS/PIP methodology is straightforwardly extended to multivariable systems [e.g. 15], this has not proven necessary in the present case. In fact, as discussed in Section 4.6, simple rules are implemented to switch between the two algorithms.

4.1 Non-Minimal State-Space (NMSS) form

It is easy to show that the model (1) can be represented by the following NMSS equations,

$$\begin{aligned}\mathbf{x}(k) &= \mathbf{F}x(k-1) + \mathbf{g}u(k-1) + \mathbf{d}y_d(k) \\ y(k) &= \mathbf{h}\mathbf{x}(k)\end{aligned}\tag{4}$$

The $n + m$ dimensional non-minimal state vector $\mathbf{x}(k)$, so called because it is of higher dimension than conventional n th order minimal state vectors, consists of the present and past sampled values of the output variable $y(k)$ and the past sampled values of the input variable $u(k)$, i.e.,

$$\mathbf{x}(k) = \begin{bmatrix} y(k) & y(k-1) & \cdots & y(k-n+1) & u(k-1) & u(k-m+1) & z(k) \end{bmatrix}^T \quad (5)$$

where $z(k)$ is the integral-of-error between the reference or command input $y_d(k)$ and the sampled output $y(k)$, defined as follows,

$$z(k) = z(k-1) + y_d(k) - y(k) \quad (6)$$

The state transition matrix \mathbf{F} , input vector \mathbf{g} , command input vector \mathbf{d} and output vector \mathbf{h} of the NMSS system are subsequently defined below,

$$\mathbf{F} = \begin{bmatrix}
-a_1 & -a_2 & \cdots & -a_{n-1} & -a_n & b_2 & b_3 & \cdots & b_{m-1} & b_m & 0 \\
1 & 0 & \cdots & 0 & 0 & 0 & 0 & \cdots & 0 & 0 & 0 \\
0 & 1 & \cdots & 0 & 0 & 0 & 0 & \cdots & 0 & 0 & 0 \\
\vdots & \vdots & \ddots & \vdots & \vdots & \vdots & \vdots & \ddots & \vdots & \vdots & \vdots \\
0 & 0 & \cdots & 1 & 0 & 0 & 0 & \cdots & 0 & 0 & 0 \\
0 & 0 & \cdots & 0 & 0 & 0 & 0 & \cdots & 0 & 0 & 0 \\
0 & 0 & \cdots & 0 & 0 & 1 & 0 & \cdots & 0 & 0 & 0 \\
0 & 0 & \cdots & 0 & 0 & 0 & 1 & \cdots & 0 & 0 & 0 \\
\vdots & \vdots & \ddots & \vdots & \vdots & \vdots & \vdots & \ddots & \vdots & \vdots & \vdots \\
1 & 0 & \cdots & 0 & 0 & 0 & 0 & \cdots & 1 & 0 & 0 \\
a_1 & a_2 & \cdots & a_{n-1} & a_n & -b_2 & -b_3 & \cdots & -b_{m-1} & -b_m & 1
\end{bmatrix}$$

$$\mathbf{g} = \begin{bmatrix} b_1 & 0 & 0 & \cdots & 0 & 1 & 0 & 0 & \cdots & 0 & -b_1 \end{bmatrix}^T$$

$$\mathbf{d} = \begin{bmatrix} 0 & 0 & 0 & \cdots & 0 & 0 & 0 & 0 & \cdots & 0 & 1 \end{bmatrix}^T$$

$$\mathbf{h} = \begin{bmatrix} 1 & 0 & 0 & \cdots & 0 & 0 & 0 & 0 & \cdots & 0 & 0 \end{bmatrix}^T$$
(7)

Inherent type 1 servomechanism performance is introduced by means of the integral-of-error part of the state vector, $z(k)$. If the closed-loop system is stable, then this ensures that steady-state tracking of the command level is inherent in the basic design.

4.2 Proportional-Integral-Plus (PIP) control

The State Variable Feedback (SVF) control law associated with the NMSS model (4) takes the usual form,

$$u(k) = -\mathbf{k}\mathbf{x}(k) \quad (8)$$

where \mathbf{k} is the $n + m$ dimensional SVF control gain vector,

$$\mathbf{k} = \begin{bmatrix} f_0 & f_1 & \cdots & f_{n-1} & g_1 & \cdots & g_{m-1} - k_I \end{bmatrix} \quad (9)$$

In more conventional block-diagram terms, the SVF controller (8) can be implemented as shown in Fig. 4, where it is clear that it can be considered as one particular extension of the ubiquitous PI controller, in which the PI action is, in general, enhanced by the higher order forward path and feedback compensators $1/G(z^{-1})$ and $F_1(z^{-1})$, respectively, where $1/G(z^{-1})$ and $F_1(z^{-1})$ are defined as follows,

$$\begin{aligned} F_1(z^{-1}) &= f_1 z^{-1} + \cdots + f_{n-1} z^{-(n-1)} \\ G(z^{-1}) &= 1 + g_1 z^{-1} + \cdots + g_{m-1} z^{-(m-1)} \end{aligned} \quad (10)$$

However, because it exploits fully the power of SVF within the NMSS setting, PIP control is inherently much more flexible and sophisticated, allowing for well-known SVF strategies such as closed loop pole assignment,

with complete (or partial) decoupling control in the multivariable case; or optimisation in terms of a Linear-Quadratic (LQ) cost function of the form,

$$J = \frac{1}{2} \sum_{i=0}^{\infty} \{ \mathbf{x}(i) \mathbf{Q} \mathbf{x}(i) + r u^2(i) \} \quad (11)$$

where \mathbf{Q} is a $n+m$ by $n+m$ matrix and r is a scalar weight on the input.

It is worth noting that, due to the special structure of the non-minimal state vector, the elements of the LQ weighting matrices have particularly simple interpretation, since the diagonal elements directly define weights assigned to the measured variables and integral-of-error states. For example, \mathbf{Q} can be formed conveniently as a diagonal matrix with elements defined as follows,

$$\mathbf{Q} = \text{diag} \left(q_1 \quad q_2 \quad \cdots \quad q_n \quad q_{n+1} \quad \cdots \quad q_{n+m-1} \quad q_{n+m} \right) \quad (12)$$

Here, the user defined output weighting parameters q_1, q_2, \dots, q_n , and input weighting parameters $q_{n+1}, q_{n+2}, \dots, q_{n+m-1}$, are generally set equal to common values of q_y and q_u respectively; while q_{n+m} is denoted by q_e to indicate that it provides a weighting constraint on the integral-of-error state variable $z(k)$. In this ‘three term’ formulation (analogous to the conventional three-term PID controller), the input weight is defined as $r = q_u$.

The ‘default’ PIP-LQ controller is then obtained using total optimal control weights of unity, i.e., $q_y = 1/n$, $q_u = 1/m$ and $q_e = 1$. The resulting SVF

gains are obtained from the steady state solution of the well known discrete time matrix Riccati equation [e.g. 16].

In many cases, good closed loop performance is obtained by straightforward manual tuning of the diagonal LQ weights as discussed above. Alternatively, in more difficult situations, the PIP control system is ideal for incorporation within a multi-objective optimisation framework, where satisfactory compromise can be obtained between conflicting objectives such as robustness, overshoot, rise times and multivariable decoupling. This is achieved by concurrent optimisation of the diagonal and off diagonal elements of the weighting matrices in the cost function, as described by [17].

4.3 Incremental form

In practice, the PIP control law derived from Fig. 4 is always implemented in the following incremental form,

$$u(k) = u(k-1) + k_I \{y_d(k) - y(k)\} - F(z^{-1})\Delta y(k) - \{G(z^{-1}) - 1\} \Delta u(k) \quad (13)$$

where $\Delta = 1 - z^{-1}$ is the difference operator and $F(z^{-1}) = f_0 + F_1(z^{-1})$. Equation (13) is not only the most obvious and convenient for digital implementation but also provides an inherent means of avoiding ‘integral windup’

in the PIP controller. To avoid such integral wind up, which is caused by integration of control errors during periods of actuator saturation, equation (13) is employed with the following correction,

$$u(k) = \begin{cases} u_{max} & \text{when } u(k) > u_{max} \\ u_{min} & \text{when } u(k) < u_{min} \end{cases} \quad (14)$$

In this manner, $u(k)$ and its past values are kept within their practically realisable limits, represented here by u_{min} and u_{max} .

4.4 PIP control design for the axial fan

For the transfer function model (2), the NMSS form (4) is based on the definition of four state variables, i.e. $y(k)$, $u(k-1)$, $u(k-2)$ and $z(k)$. The state matrices are defined as follows,

$$\begin{aligned}
\mathbf{F} &= \begin{bmatrix} 0.4401 & 0 & 79.71 & 0 \\ 0 & 0 & 0 & 0 \\ 0 & 1 & 0 & 0 \\ -0.4401 & 0 & -79.71 & 1 \end{bmatrix} \\
\mathbf{g} &= \begin{bmatrix} 0 & 1 & 0 & 0 \end{bmatrix}^T \\
\mathbf{d} &= \begin{bmatrix} 0 & 0 & 0 & 1 \end{bmatrix}^T \\
\mathbf{h} &= \begin{bmatrix} 1 & 0 & 0 & 0 \end{bmatrix}^T
\end{aligned} \tag{15}$$

The default PIP-LQ design with $q_y = 1$, $q_u = 1$ and $q_e = 1$ (see Section 4.2) yields a rather fast response that is not sufficiently robust to model uncertainty and the inherent non-linearity's in the system.

However, experimentation quickly reveals that reducing the weighting on the integral-of-error state variable by a factor of 10 ($q_e = 0.1$) provides a satisfactory closed loop response across a wide range of operating conditions. In this case, the control gain vector (9) is defined as follows,

$$\mathbf{k} = \begin{bmatrix} 0.0032 & 0.7102 & 0.5827 & -0.0034 \end{bmatrix} \tag{16}$$

while the incremental form is obtained by substituting these gains into equation (13) as shown below,

$$\begin{aligned}
u(k) = & u(k-1) + 0.0034 \{y_d(k) - y(k)\} - 0.0032 \{y(k) - y(k-1)\} \\
& - 0.7102 \{u(k-1) - u(k-2)\} - 0.5827 \{u(k-2) - u(k-3)\}
\end{aligned}
\tag{17}$$

Finally, the correction (14) is employed for the on-line implementation, limiting the applied voltage to the range $u_{min} = 20\%$ to $u_{max} = 100\%$. Note that when u_{min} falls to 20%, the throttling valve controller is activated and the main fan held constant at this voltage.

As described by reference [10], the PIP controller given by equation (17) provides good control for mid to high ventilation rates. The results in the former paper show that it offers noticeable improvements over an equivalent PID design, especially for the more extreme ventilation rates away from the design operating point. Furthermore, the PIP algorithm proves considerably more robust to realistic pressure disturbances.

However, at low ventilation rates, the control performance of both the PID and PIP algorithms is sometimes poor. This was the motivation for the earlier development of a scheduled gain, PIP control system utilising the throttling valve, also described by [10]. In this case, fixing the valve at 60% closed when the ventilation rate drops below 1000m³/h yields improved control, albeit for greater operating costs. By contrast, the present paper considers the design of an active throttling valve controller for directly regulating the ventilation

rate below $1000\text{m}^3/\text{h}$, as discussed below.

4.5 PIP control design for the throttling valve

The PIP controller for the throttling valve is designed in a similar manner to that of the axial fan above. In this case, the transfer function model (3) is represented in NMSS form (4) using the following state matrices,

$$\begin{aligned} \mathbf{F} &= \begin{bmatrix} 0.7301 & 0 & -3.63 & 0 \\ 0 & 0 & 0 & 0 \\ 0 & 1 & 0 & 0 \\ -0.7301 & 0 & 3.63 & 1 \end{bmatrix} \\ \mathbf{g} &= \begin{bmatrix} 0 & 1 & 0 & 0 \end{bmatrix}^T \\ \mathbf{d} &= \begin{bmatrix} 0 & 0 & 0 & 1 \end{bmatrix}^T \\ \mathbf{h} &= \begin{bmatrix} 1 & 0 & 0 & 0 \end{bmatrix}^T \end{aligned} \tag{18}$$

A reduced integral-of-error state weighting of $q_e = 0.01$, yields a PIP-LQ design with the best disturbance rejection response across a wide range of operating conditions. Here, the control gain vector is defined as follows,

$$\mathbf{k} = \begin{bmatrix} -0.1318 & 0.7757 & 0.6567 & 0.0248 \end{bmatrix} \tag{19}$$

while the incremental form is, therefore,

$$\begin{aligned}
u(k) = & u(k-1) - 0.0248 \{y_d(k) - y(k)\} + 0.1318 \{y(k) - y(k-1)\} \\
& - 0.7757 \{u(k-1) - u(k-2)\} - 0.6567 \{u(k-2) - u(k-3)\}
\end{aligned}
\tag{20}$$

Again, the correction shown by equation (14) is employed, this time limiting the applied voltage to the range 20% to 95%, where the maximum limit ensures that the valve does not entirely block the airflow by closing completely. In this case, the 20% lower limit provides a degree of hysteresis in the final design, as discussed in Section 4.6.

Prior to implementation, standard deterministic evaluation tools such as the transient (step) and frequency response characteristics are combined with Monte Carlo (MC) simulation analysis [13] to assess the robustness and sensitivity of this new throttling valve control algorithm (Fig. 5). In MC analysis, an estimate of the covariance matrix $\mathbf{P}^*(k)$ provided by the SRIV estimation procedure is utilised to generate a number of closed-loop stochastic realisations, which are then evaluated to ensure that the control design is acceptably robust to this level of uncertainty.

In fact, for the purposes of Fig. 5, the parametric uncertainty was artificially *increased* by a factor of 50 to better illustrate the Monte Carlo envelope. Nonetheless, the Nyquist traces for all of the MC realisations are well to the right of the critical '-1' point, implying that the control system

yields highly stable responses despite the simulated parametric uncertainty. Similarly, it is clear that all of the closed-loop pole positions (or stochastic root loci) are well inside the unit circle on the complex z -plane. Finally, note that although just 100 realisations are employed in the figure, the results change insignificantly if more realisations (1000) are utilised.

4.6 Combined fan/valve controller

The new fan/valve PIP control system features simple rules to switch between the two algorithms (17) and (20). For mid to high ventilation rates, the throttling valve is held fully open to minimise operating costs. However, for low ventilation rates or during particularly strong disturbances, control switches to the throttling valve. In particular, the axial fan voltage is held constant at 20% when the control input determined by (17) would otherwise fall below this threshold. At this point, the throttling valve becomes the control actuator using (20).

Similarly, when the applied voltage to the throttling valve falls to 20%, the valve is immediately opened fully and the axial fan controller (17) reactivated. This transition from throttling valve to fan control inherently includes a degree of hysteresis, which stops undesirable switching between the two algorithms when the ventilation rate is close to $1000\text{m}^3/\text{h}$. Finally, note that

both algorithms utilise specially developed initialisation settings to ensure a smooth transition between them [18].

As illustrated by Fig. 6, the approach works extremely well in practice. Here, the bottom graph shows the fluctuating control signals of both the fan and the throttling valve, as the ventilation rate is successfully maintained at a number of operating levels. Fig. 7 shows the equivalent power consumption and applied voltage to the disturbance fan. Note that power consumption is based on the axial fan voltage, since the throttling valve consumes comparatively little power for its operation. As discussed in Section 2, the disturbance fan represents realistic pressure variations.

5 Control evaluation

The present section compares the performance and operating costs of the PIP controller above, with an equivalent commercial design also implemented on the Leuven ventilation chamber. Here, the commercial controller is based on a PID algorithm combined with a number of *ad hoc* rules for adjustment of the throttling valve.

For ventilation rates in the region of $3000\text{m}^3/\text{h}$, the PIP and commercial designs behave in a similar fashion, although the latter appears to respond slightly slower to changes in the set point. For the highest ventilation rates

Table 1: Control performance and operating costs.

Controller	Parameter	Mean	Std. Dev.
NMSS/PIP	airflow	602m ³ /h	36.9m ³ /h
Commercial	airflow	597m ³ /h	7.8m ³ /h
NMSS/PIP	power	81W	0.7W
Commercial	power	150W	2.4W

or strong disturbance inputs, the PIP design is found to be more robust than the commercial algorithm. This latter result is similar to that discussed in reference [10] and so, for brevity, is not illustrated here.

However, it is low ventilation rates that are of most interest to the present paper. In this regard, consider Table 1, which compares the mean and standard deviation of the ventilation rate (for a set point of 600m³/h) and power consumption of the NMSS-based PIP combined fan/valve and commercial controllers. Table 1 shows a considerable reduction in power consumption for the PIP controller, from an average of 150W to just 81W.

Although the commercial controller has improved noise variance properties when compared with the PIP design, as shown by the final column of Table 1, this occurs simply because the commercial controller closes the throttling valve by a larger degree, reducing the noise encountered by the ventilation rate sensor. This is necessary in order to stabilise the distur-

bance response of the PID algorithm, but is not required in the PIP case. This restricted airflow associated with the commercial controller inevitably requires a higher applied voltage to the axial fan, resulting in the higher operating cost. Furthermore, it should be pointed out that, in absolute terms, the PIP controller performs very well indeed, as is clear from Fig. 6, well within the performance requirements of a microclimate control system.

Finally, note that the previously developed, gain scheduled, PIP algorithm [10], has similar power consumption characteristics to that of the commercial controller. In this regard, the main advantage of the new combined fan/valve PIP approach, is the reduced operating cost illustrated by Table 1.

For all the experiments discussed above, the disturbance fan operates against the flow of air generated by the axial fan. However, by reinstalling the disturbance fan in the reverse direction, it may be used to simulate the effect of any natural ventilation present in the system. As discussed in Section 2, such natural ventilation has the potential for further reducing the power consumption of the axial fan.

The obvious advantage of the new fan/valve control configuration in this context, is that the system automatically switches to throttling valve control when the axial fan is not required. Preliminary results in this regard are promising and offer the potential for further cost savings [18]. Current research is concerned with evaluating the robustness and performance of such

an approach under a wide range of operating conditions, and this will be reported in future publications.

6 Conclusion

This paper is concerned with Proportional-Integral-Plus (PIP) control of ventilation rate in mechanically ventilated agricultural buildings. In particular, the paper considers the design of a combined fan and throttling valve control system for a 22m³ ventilation test chamber at the Katholieke Universiteit Leuven, representing a section of a livestock building or glasshouse. In this case, PIP controllers are developed for both the axial fan and a throttling valve, where the latter is introduced to stabilise the airflow at low ventilation rates.

For these experiments, separate PIP algorithms are designed and implemented for both control actuators, using simple rules to switch between the controllers as appropriate. This straightforward arrangement proves to work very well in practice, as illustrated by Fig. 6. In particular, the fan/valve PIP design yields significant reductions in power consumption when compared to both a previously developed scheduled PIP design and a commercial controller also optimised for the test chamber.

On the basis of the experiments discussed above, extrapolating the re-

duced operating cost of the new PIP ventilation controller to the total production costs per housed animal, would yield significant savings. This clearly makes the PIP algorithm a viable proposition, since the control implementation complexity is no greater than that of the PID-based commercial design presently employed.

Acknowledgments

The authors are grateful for the support of the Engineering and Physical Sciences Research Council (EPSRC). This publication is expanded and updated from reference [19], first presented at the 16th International Conference on Systems Engineering (ICSE).

References

- [1] G. A. Carpenter. Ventilation of buildings for intensively housed livestock. In J. L. Montieth and L. E. Mont, editors, *Heat loss from animals and man*, pages 389–403. Butterworths, London, 1974.
- [2] J. M. Randall. Ventilation system design. In J. A. Clark, editor, *Environmental aspects of housing for animal production*, pages 351–369. Butterworths, London, 1981.

- [3] A. J. Hebner, C. R. Boon, and G. H. Peugh. Air patterns and turbulence in an experimental livestock building. *Journal of Agricultural Engineering Research*, 64:209–226, 1996.
- [4] E. Vranken. *Analysis and Optimisation of Ventilation Control in Livestock Buildings*. PhD thesis, Katholieke Universiteit Leuven, Belgium, 1999.
- [5] P. F. Davis and A. W. Hooper. Improvement of greenhouse heating control. *IEE Proceedings - Control Theory and Applications*, 138:249, 1991.
- [6] N. Sigrimis, K. G. Arvanitis, I. K. Kookos, and P. N. Paraskevopoulos. H-infinity-pi controller tuning for greenhouse temperature control. In *IFAC 14th Triennial World Congress*, Beijing, China, 1999.
- [7] C. J. Taylor, P. C. Young, and A. Chotai. State space control system design based on non-minimal state-variable feedback : Further generalisation and unification results. *International Journal of Control*, 73:1329–1345, 2000.
- [8] P. C. Young, M. A. Behzadi, C. L. Wang, and A. Chotai. Direct digital and adaptive control by input-output, state variable feedback pole assignment. *International Journal of Control*, 46:1867–1881, 1987.

- [9] L. Price, P. C. Young, D. Berckmans, K. Janssens, and C. J. Taylor. Data-based mechanistic modelling (dbm) and control of mass and energy transfer in agricultural buildings. *Annual Reviews in Control*, 23:71–83, 1999.
- [10] C. J. Taylor, P. Leigh, L. Price, P. C. Young, D. Berckmans, K. Janssens, E. Vranken, and R. Gevers. Proportional-integral-plus (pip) control of ventilation rate in agricultural buildings. *Control Engineering Practice*, 12:225–233, 2004.
- [11] A. P. Robertson and A. G. Glass. The silsoe structures building - its design, instrumentation and research facilities. Divisional note, AFRC Institute of Engineering Research, Wrest Park, Silsoe, Bedford, UK, 1988.
- [12] P. C. Young. *Recursive Estimation and Time Series Analysis*. Springer-Verlag, Berlin, 1984.
- [13] P. C. Young. Simplified refined instrumental variable (sriv) estimation and true digital control (tdc): a tutorial introduction. In *1st European Control Conference*, pages 1295–1306, Grenoble, 1991.
- [14] P. C. Young and A. J. Jakeman. Refined instrumental variable meth-

- ods of recursive time-series analysis, part 3: extensions. *International Journal of Control*, 31:741–764, 1980.
- [15] P. C. Young, M. Lees, A. Chotai, W. Tych, and Z. S. Chalabi. Modelling and pip control of a glasshouse micro-climate. *Control Engineering Practice*, 2(4):591–604, 1994.
- [16] K. J. Astrom and B. Wittenmark. *Computer controlled systems: theory and design*. Information and system sciences series. Prentice-Hall, 1984.
- [17] A. Chotai, P. C. Young, P. McKenna, and W. Tych. Pip design for delta-operator systems: Part 2, mimo systems. *International Journal of Control*, 70:149–168, 1998.
- [18] P. A. Leigh. *Modelling and Control of Micro-Environmental Systems*. PhD thesis, Institute of Environmental and Natural Sciences, Lancaster University, UK, 2002.
- [19] P. Leigh, C. J. Taylor, A. Chotai, P. C. Young, and E. Vranken. Implementation of a combined fan and valve control design in a ventilation chamber. In K. J. Burnham and O. C. L. Haas, editors, *16th International Conference on Systems Engineering*, pages 423–428, Coventry University, UK, September 2003.

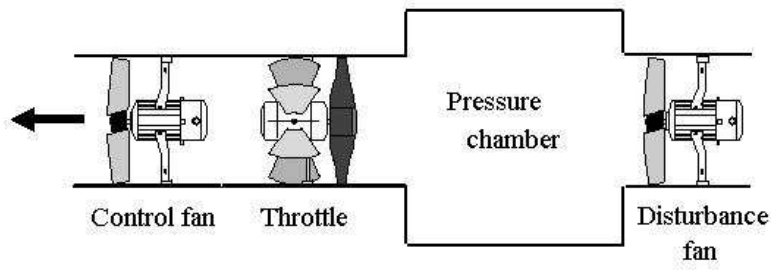


Figure 1: Schematic layout of the ventilation rate test chamber.

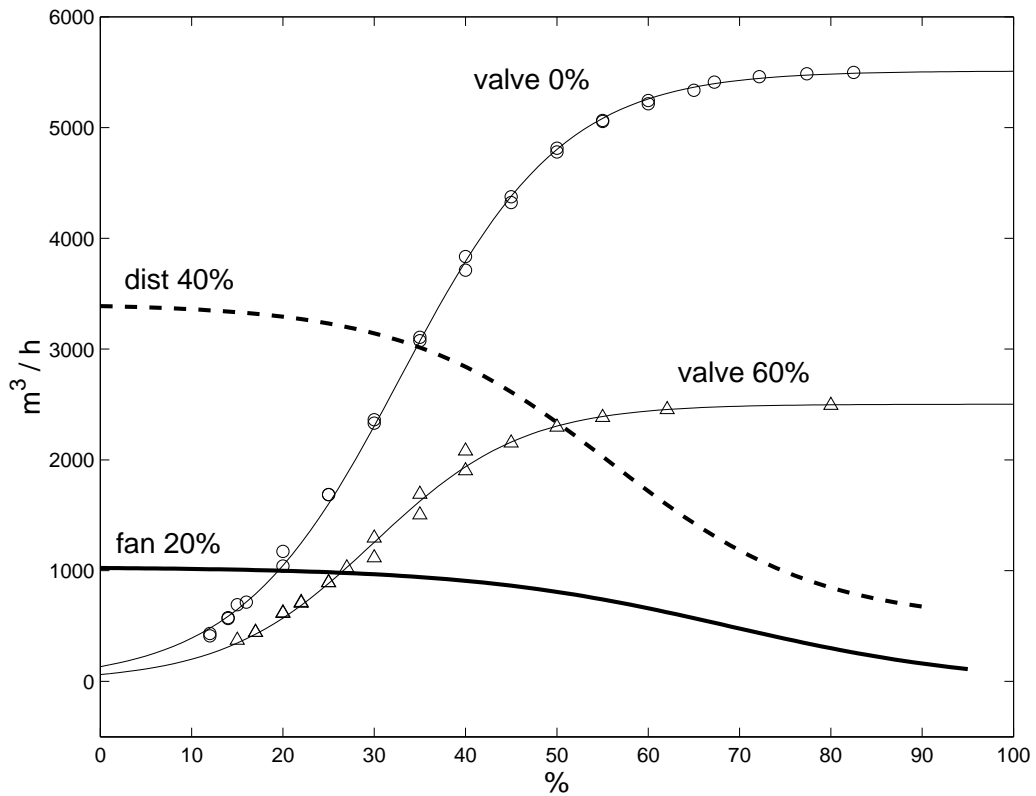


Figure 2: Steady state power curves. Thin traces: airflow rate plotted against control fan applied voltage for two different throttling valve settings, fully open (circles) and 60% closed (triangles). Thick traces: airflow plotted against throttling valve applied voltage, for control fan 20% (solid trace) and disturbance fan 40% (dashed).

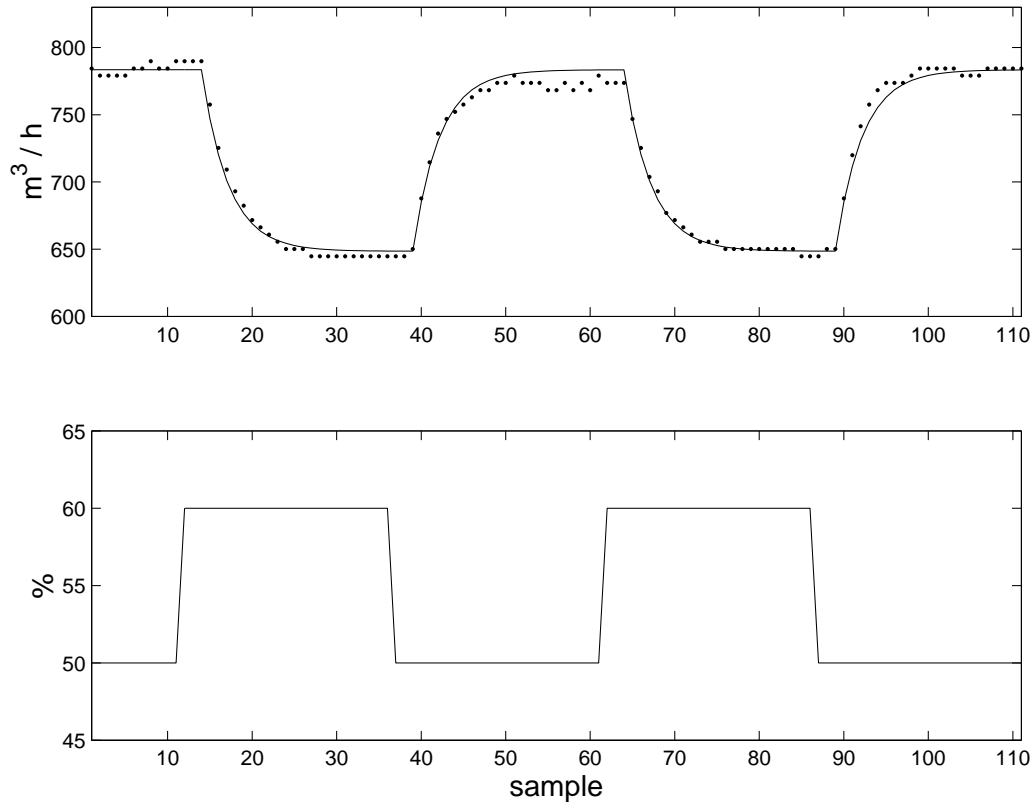


Figure 3: Open loop throttling valve experiment. Ventilation rate (dots; top graph) and response of the identified model (3), together with the applied voltage to the throttling valve (bottom graph), all plotted against sample number.

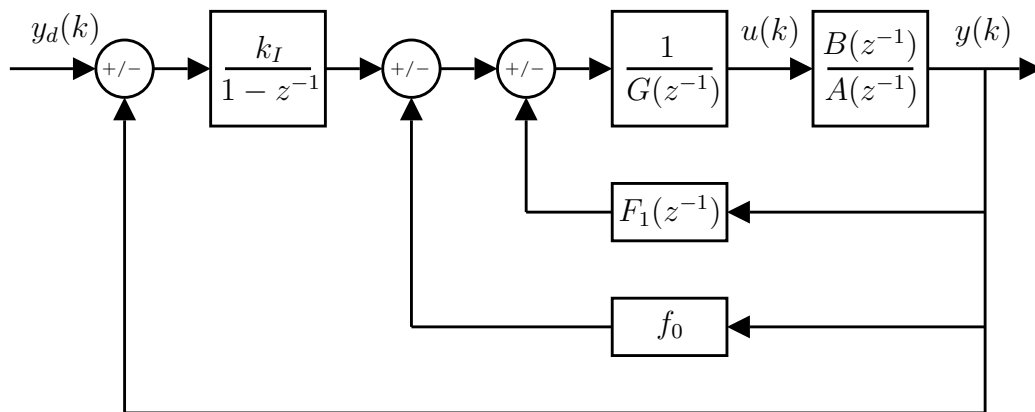


Figure 4: PIP control implemented in feedback form.

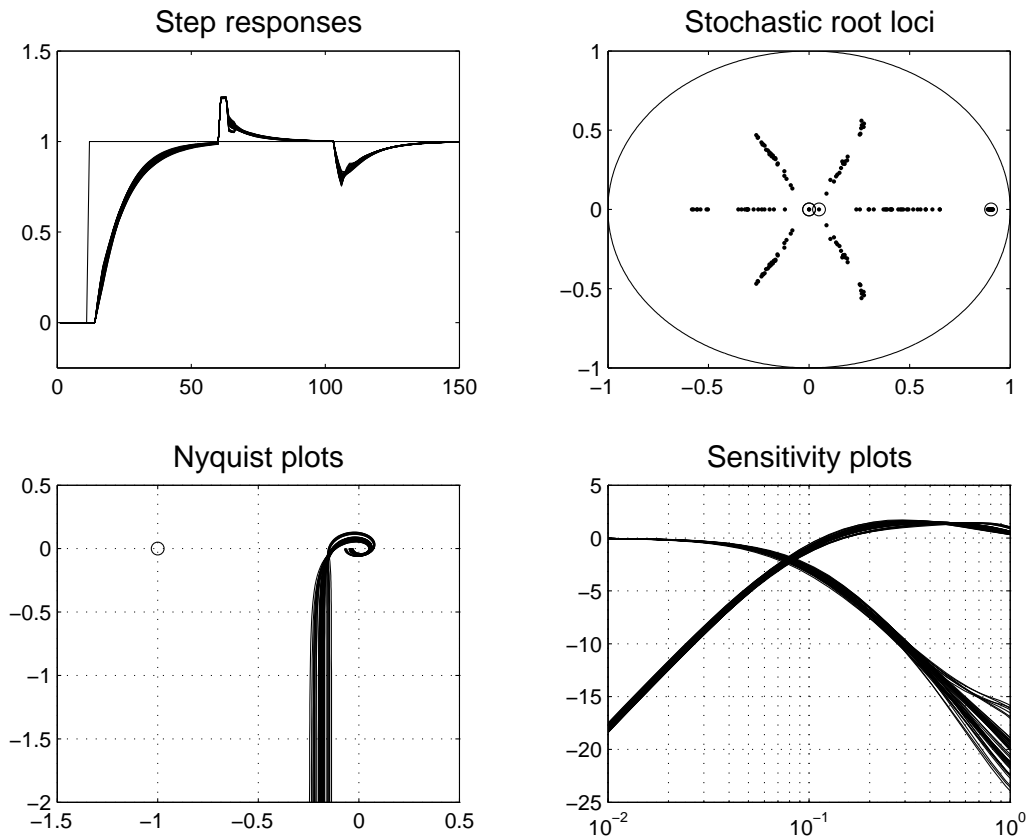


Figure 5: Monte Carlo evaluation (100 realisations) of the throttling valve controller (20), based on the estimated parametric uncertainty associated with the model (3). Clockwise from top left: (a) response to a step change in the set point with load and input disturbances of 0.25 (60th sample) and 0.025 (100th sample) respectively; closed loop pole positions plotted on the complex z -plane, with the design poles highlighted by circles; Nyquist plot with the imaginary component of the transfer function plotted against the real component; and, finally, the sensitivity and complementary sensitivity functions (dB) plotted against frequency (rads/sec).

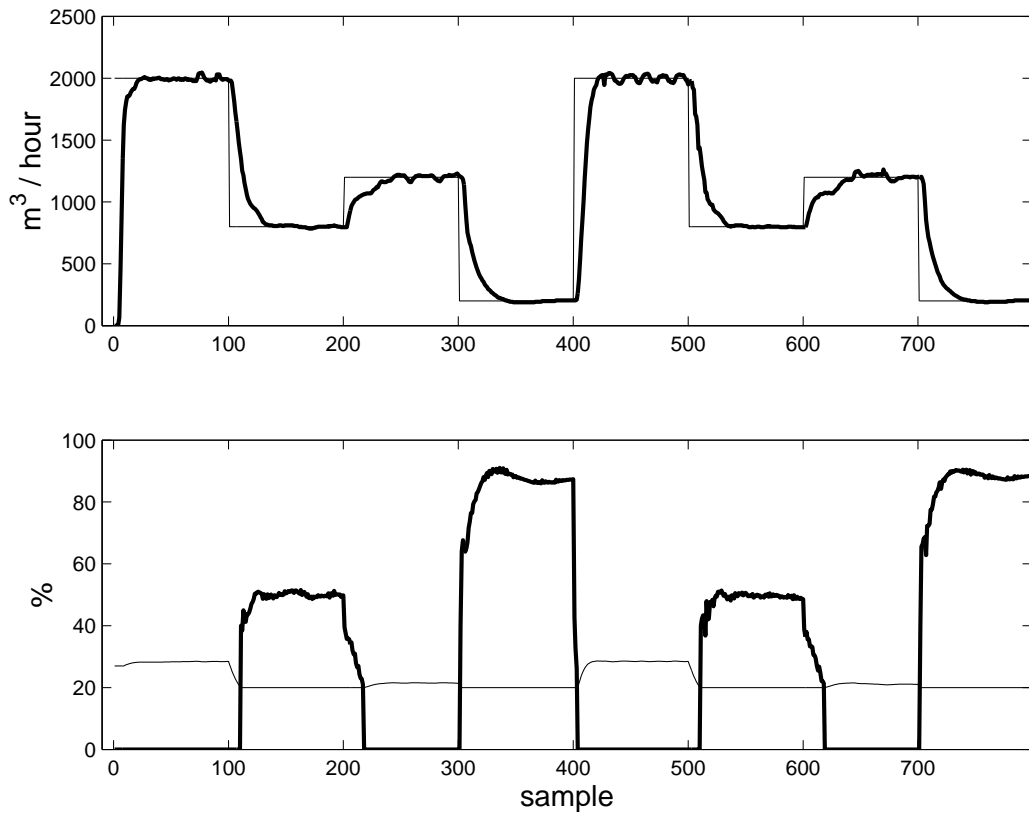


Figure 6: Response of the fan/valve controller. Ventilation rate (thick trace) and set point (top graph), together with the applied voltage to the throttling valve (thick trace) and axial fan (bottom graph), all plotted against sample number.

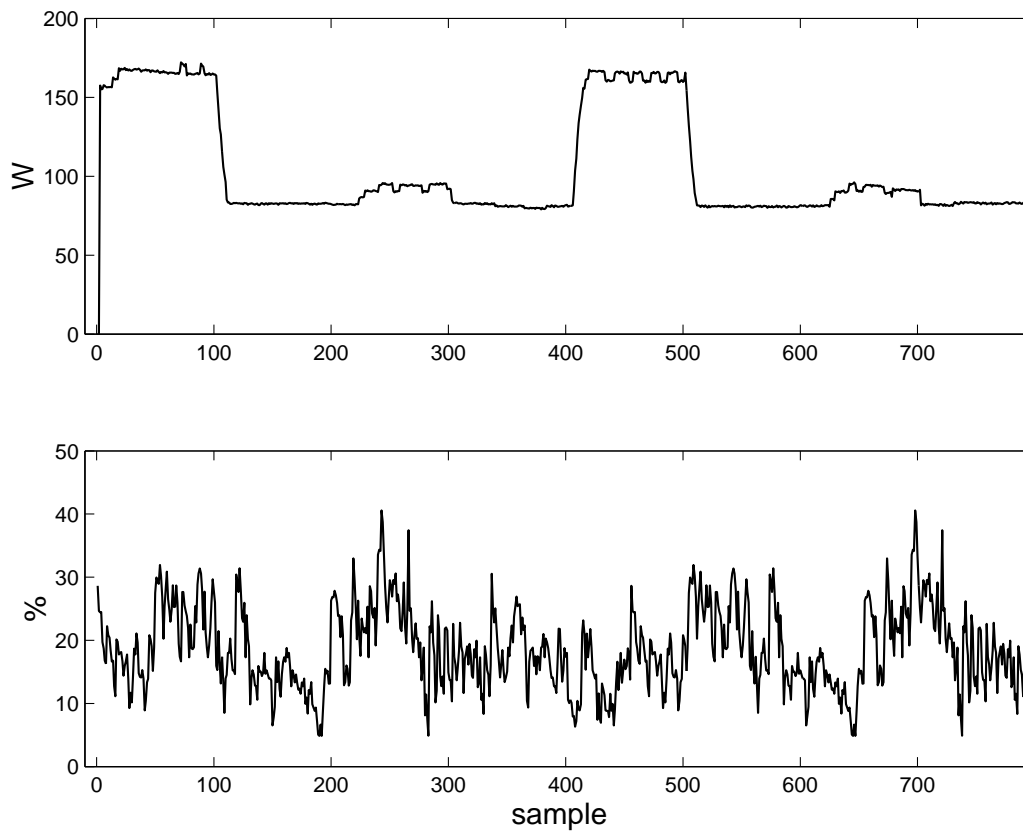


Figure 7: Power consumption (top graph) and applied voltage to the disturbance fan (bottom graph) for the response in Fig. 6.